Journal of Theoretical and Applied Mechanics, Sofia, Vol.53 (2023) pp. 319-347
FLUID MECHANICS

STABILITY OF LIQUID-VAPOR INTERFACE AT STEADY-STATE EVAPORATION AND CONDENSATION

K.D. DANOV*

Department of Chemical and Pharmaceutical Engineering,
Faculty of Chemistry and Pharmacy, University of Sofia,
1 James Bourchier Ave., 1164 Sofia, Bulgaria

[Received: 1 August 2023. Accepted: 5 October 2023]

doi: https://doi.org/10.55787/jtams.23.53.4.319

ABSTRACT: The aim of this study is to perform a stability analysis of a thermo-capillary flow in a steady-state evaporating/condensing liquid layer applying the statistical rate theory expression for the mass flux across the interface. In the general mass, momentum and energy balance equations, the effects of gravity, temperature gradients in the surface tension, the interfacial momentum and energy loss due to the net mass flux are taken into account. Assuming a non-deformable surface and low dynamic viscosity and thermal conductivity of the vapor, the stability problem of the liquid phase is separated from that for the vapor. The exact solution is found and the dispersion relationship is solved numerically for water. The numerical results show that the interfacial instability mode always takes place in spite of the direction of the mass flux across the interface. The main physical reason for this kind of instability is the strong dependence of the mass flux on the vapor pressure predicted from the statistical rate theory. Other internal instability modes are described as a function of the Rayleigh and Marangoni numbers. The stability diagrams are discussed in the light of the available experiments for controllable water steady-state evaporation and condensation.

KEY WORDS: stability of liquid-vapor interface, evaporation and condensation, interfacial turbulence, statistical rate theory, mass flux across the interface.

1 INTRODUCTION

The phenomena of convection cells observed by Bénard [1], when a horizontal layer of liquid is heated from below, was explained by Rayleigh [2] in terms of buoyancy. Rayleigh's analysis was extended and refined by later authors and a good qualitative agreement with experiments involving marginal stability was reported [3–6]. In all these treatments, the force causing the layer instability was only buoyancy – when

*Corresponding author e-mail: KD@LCPE.Uni-Sofia.Bg

the lighter liquid is above the heavier, the mentioned instability takes place yielding the Bénard cellular convection [1]. Pearson [7] and Nield [8] offered an explanation for instability with a similar cellular motion – when the upper surface is free then Bénard-type cells could be produced also by tractions arising from the variation of surface tension with temperature. Sternling and Scriven [9] considered the case of two semi-infinite liquid layers separated by non-deformable interface. They showed that overstability and wave motions are possible in particular if the heat transfer occurs from the phase with higher kinematic viscosity and thermal diffusivity. Rednikov et al. [10] reported a complete numerical analysis of the Nield problem, including the oscillatory marginal stability diagrams.

In the case of liquid-vapor interface, the latent heat required for evaporation is balanced by the heat flux across the liquid interface and in this way a high temperature in both phases can be maintained. New modes of instability appear at an evaporating/condensing liquid-vapor surface [11–16]. The authors [13–16] examined the hydrodynamic stability of a pure liquid undergoing steady rapid evaporation. Their results showed that because of the rapid evaporation, the liquid-vapor interface is unstable to: local variations in evaporation rate; local surface depressions being produced by the force exerted on the surface by the rapidly departing vapor; sustained liquid flows being driven by the resulting shear exerted on the liquid surface by the vapor. Later experimental results [17] and detailed stability analysis [18–20] confirmed these conclusions regarding the various courses of instabilities. The role of surfactants in damping the wave growth and the stabilizing and destabilizing effects of different types of surface force for very thin liquid layers were also examined [21–26].

Many authors [13–16, 18–26] assumed that: the temperatures of the liquid and vapor at the interface are equal; the evaporation/condensation mass flux is related to the properties of liquid through the Hertz-Knudsen [27] equation; the Neumann-type boundary condition at the interface relates the heat flux and the temperature difference to a given constant heat transfer coefficient κ_s. Huang and Joseph [28, 29] were the first to address the problem of the influence of phase change and thermodynamic conditions at the evaporating interface on the stability of convective flows in liquid-vapor systems. The experiments [30–36] show that there is a temperature discontinuity of several degrees between the liquid and vapor temperatures at the interface of pure substances. Shankar and Deshpande [30] measured the temperature profiles in the vapor and liquid of evaporating mercury – the temperature jumps at the interface can be as large as almost 50% of the applied temperature differences. In experimental studies [31–36] of the conditions at the interface during steady-state evaporation or condensation, a temperature discontinuity at the interface has been found in which the temperature in the vapor is greater than that in the liquid during either evaporation or condensation. During evaporation such a discontinuity has

been found for each of three different liquids: water, octane and methylcyclohexane. The magnitude of the discontinuity increases as the phase change rate increases. To understand this phenomenon, different methods of calculating evaporation and condensation mass fluxes and the temperature discontinuities at liquid-vapor interfaces are used in the literature.

In the framework of the classical kinetic theory, Pao [37,38] was the first to predict the temperature inversion in the vapor phase. All subsequent treatments [30, 39–41] show that the vapor close to the evaporating surface would be supersaturated under the same conditions as those leading to the inverted temperature profile. The calculated transfer coefficients for evaporation from experiments [42, 43] are smaller by a factor of 30-100 than those calculated from the classical kinetic theory. If one considers the equilibrium exchange of particles between a liquid and vapor in molecular dynamics simulations [44], one observes the occurrence of small clusters of particles in the vapor close to the surface and a small region with a low density in the liquid contiguous phase. Computer simulations in the non-equilibrium molecular dynamics of the steady-state heat and mass transport in condensation [45, 46] show that the use of classical kinetic theory derived for monoatomic fluids is questionable for polyatomic fluids.

The problem of the boundary conditions at the interface at slow evaporation or condensation rates was also examined in the context of non-equilibrium thermodynamics for two-phase systems [42, 43]. Bedeaux et al. [42] derived an expression for the excess entropy production in the interfacial region and proved that the temperature of the interface may be different from the temperatures of the contiguous liquid and vapor phases. Therefore, the interface appears as a phase with different thermodynamic parameters (enthalpy, chemical potential, etc.) compared with the adjusted liquid and vapor phases. The matrix of Onsager transfer coefficients is calculated from classical kinetic theory [42] and directly from yhe experiments of liquid evaporation [43].

A more adequate way of interpreting experimental data is the development and application of the statistical rate theory (SRT) [32–34, 36]. Note that SRT predicts directly the mass flux in the studied system without an assumption of quasi-equilibrium. Based on the complete expressions for predicting liquid evaporation or condensation flux [32], the experimental data for water, octane and methylcyclohexane are explained [33, 34, 36] without any adjustable parameter. Ward [48] proves that SRT does not contradict results obtained in non-equilibrium thermodynamics – the excess entropy production in the interfacial region calculated from SRT is always positive.

This paper is organized as follows. In Section 2, the general mass, momentum, and energy balance equations in the bulk and at the liquid-vapor interface are briefly discussed. The simplification of the statistical rate theory expression for the mass flux

is reported. The problem is not closed because of the missing boundary condition for the temperature jump at the interface. In Section 3, the linear stability analysis is developed on the basis of steady-state evaporation/condensation of a semi-infinite liquid layer. Because of the smaller dynamic viscosity and thermal conductivity of the vapor phase, only the fluctuations in the vapor phase pressure appear in the boundary conditions and in the expression for mass flux. An additional assumption that the interface is non-deformable gives possibility to separate the problem of stability of the liquid phase from that of the vapor phase. The respective dispersion relationship is derived. The numerical solution of the dispersion relationship for pure water under experimental conditions [31–36] is described in Section 4.

2 General Mathematical Formulation

The density, pressure, temperature, velocity, internal energy, and heat flux of the bulk phase are denoted by ρ_α, p_α, T_α, $\mathbf{v}_\alpha$, u_α, and $\mathbf{q}_\alpha$ ($\alpha = \mathrm{L}, \mathrm{V}$). The subscripts L and V indicate the values of the respective parameters in the liquid and vapor phases. The general mass, momentum and energy balance equations for simple fluids are as follows [49, 50]:

$$\frac{\partial \rho_\alpha}{\partial t} + \nabla \cdot (\rho_\alpha \mathbf{v}_\alpha) = 0\,, \tag{1}$$

$$\frac{\partial}{\partial t}(\rho_\alpha \mathbf{v}_\alpha) + \nabla \cdot (\rho_\alpha \mathbf{v}_\alpha \mathbf{v}_\alpha) = \nabla \cdot (-p_\alpha \mathbf{I} + \mathbf{V}_\alpha) + \rho_\alpha \mathbf{g}\,, \tag{2}$$

$$\begin{aligned} \frac{\partial}{\partial t}[\rho_\alpha(\frac{v_\alpha^2}{2} - \mathbf{g}\cdot\mathbf{r} + u_\alpha)] + \nabla \cdot [\rho_\alpha \mathbf{v}_\alpha(\frac{v_\alpha^2}{2} - \mathbf{g}\cdot\mathbf{r} + u_\alpha)] \\ = \nabla \cdot [-p_\alpha \mathbf{v}_\alpha + \mathbf{V}_\alpha \cdot \mathbf{v}_\alpha - \mathbf{q}_\alpha]\,, \end{aligned} \tag{3}$$

where t is time, ∇ is the spatial gradient operator, $\mathbf{I}$ is the spatial idem factor, $\mathbf{r}$ is the vector of coordinates, $\mathbf{V}_\alpha$ is the viscous stress tensor, and $\mathbf{g}$ is the gravity acceleration.

The simplest linear laws for the viscous stress tensors and the heat fluxes are widely used in the literature for modeling the bulk fluid properties. Thus the viscous stress tensor depends on the dynamic shear and dilatational viscosities, $\eta_\alpha^{\mathrm{sh}}$ and $\eta_\alpha^{\mathrm{dil}}$, and the heat flux is a linear function of thermal conductivity κ_α ($\alpha = \mathrm{L}, \mathrm{V}$) [49, 50]:

$$\mathbf{V}_\alpha = \eta_\alpha^{\mathrm{sh}}[\nabla \mathbf{v}_\alpha + (\nabla \mathbf{v}_\alpha)^{\mathrm{tr}}] + (\eta_\alpha^{\mathrm{dil}} - \frac{2}{3}\eta_\alpha^{\mathrm{sh}})(\nabla \cdot \mathbf{v}_\alpha)\mathbf{I}\,, \tag{4}$$

$$\mathbf{q}_\alpha = -\kappa_\alpha \nabla T_\alpha\,, \tag{5}$$

where the superscript tr denotes transposition.

Assuming the Boussinesq approximation to be valid, the liquid phase is considered to be an *incompressible fluid*. Hence the density is a known function of the

temperature, $\rho_{\rm L} = \rho_{\rm L}(T_{\rm L})$, and the change of the internal energy is proportional to the change of temperature, $\mathrm{d}u_{\rm L} = c_{\rm L}^{v}\mathrm{d}T_{\rm L}$, where $c_{\rm L}^{v}$ is the heat capacity at a constant volume.

The vapor phase is modeled as an ideal gas with the heat capacities at constant pressure and volumes, $c_{\rm V}^{p}$ and $c_{\rm V}^{v}$, respectively. Therefore, the pressure, p_V, and the internal energy, u_V, are related to the density, ρ_V, and temperature, T_V, through the well-known expressions $p_{\rm V} = (c_{\rm V}^{p} - c_{\rm V}^{v})\,\rho_{\rm V}\,T_{\rm V}$ and $u_{\rm V} = c_{\rm V}^{v}\,T_{\rm V}$.

To close the system of equations (1)–(5), boundary conditions at the liquid-vapor interface and constitutive laws for the material interface are needed.

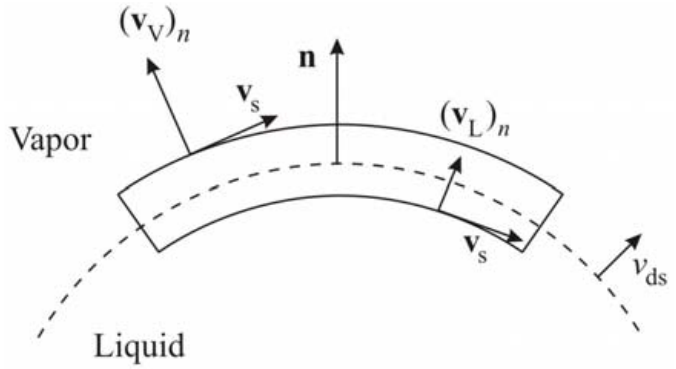

Fig. 1: Material interface and mathematical dividing surface: $(\mathbf{v}_{\rm L})_n$, $(\mathbf{v}_{\rm V})_n$, and $\mathbf{v}_s$ are the normal and tangential components of the fluid velocity at the interface and $v_{\rm ds}$ is the velocity of the dividing mathematical surface.

The material liquid-vapor interface is represented in calculations by the mathematical dividing surface with unit normal $\mathbf{n}$ pointing to the vapor phase and velocity $v_{\rm ds}$ (Fig. 1). The fluid velocities are projected to the normal and tangential directions of the dividing surface and the normal components are $(\mathbf{v}_{\rm L})_n$ and $(\mathbf{v}_{\rm V})_n$, respectively. For viscous phases, the tangential components of velocity are continuous across the interface and equal to $\mathbf{v}_s$. The general equation of the dividing surface [51, 52] can be written as $F(t, \mathbf{r}) = 0$ and the velocity $v_{\rm ds}$ is calculated from the expression $|\nabla F| v_{\rm ds} = \partial F/\partial t$. The balance of mass at the interface defines the mass flux, j, and leads to the following boundary condition [51, 52]:

$$\rho_{\rm L}(\mathbf{v}_{\rm L}\cdot\mathbf{n} - v_{\rm ds}) = \rho_{\rm V}(\mathbf{v}_{\rm V}\cdot\mathbf{n} - v_{\rm ds}) = j\,. \tag{6}$$

The evaporation mass flux is defined to be positive ($j > 0$) and the condensation mass flux is negative ($j < 0$). In the absence of mass flux across the interface, equation (6) reduces to the kinematic boundary condition.

The boundary condition for the conservation of surface excess linear momentum reads [51, 52]

$$\langle \mathbf{V}_\alpha \cdot \mathbf{n} - (p_\alpha + \frac{j^2}{\rho_\alpha})\mathbf{n} \rangle = \nabla_s \sigma + 2H\sigma\mathbf{n}\,. \tag{7}$$

Here $\langle \cdots \rangle \equiv (\cdots)_{\mathrm{L}} - (\cdots)_{\mathrm{V}}$ is the difference between the respective physical parameters calculated at the contiguous to the interface bulk liquid and vapor phases, ∇_s is the surface gradient operator, σ is the surface tension, and H is the mean curvature of the dividing surface. The right-hand side of equation (7) accounts for the capillary pressure and the Marangoni tangential surface force. In the case of pure liquid phases, the surface viscosity is negligible and the surface tension, σ, becomes the only operative surface force [50, 53]. The term j^2/ρ_α accounts for the so-called "interfacial momentum loss" due to the mass transfer across the interface. For pure fluid phases, the surface tension depends only on the temperature of liquid phase at the interface $T_{\mathrm{L}0}$, i.e. $\sigma = \sigma(T_{\mathrm{L}0})$. Hence the interfacial temperature gradient produces surface gradient of σ and gives rise to the interfacial thermo-capillary convection.

The heat capacity of the material interface is so small that conservation of energy across the interface takes place [51, 52]:

$$\left\langle \frac{j^3}{2\rho_\alpha^2} + jh_\alpha + \mathbf{q}_\alpha \cdot \mathbf{n} - \frac{j}{\rho_\alpha}\mathbf{n} \cdot \mathbf{V}_\alpha \cdot \mathbf{n} \right\rangle = 0\,, \tag{8}$$

where h_α (α = L, V) are the enthalpies of adjusted bulk phases. Equation (8) expresses that the total flux of energy, which is the sum of the kinetic energy and the thermal energy fluxes, the heat flux and the flux of energy due to the viscous friction, is continuous across the interface.

Boundary conditions (6)–(8) close the fluid dynamic problem for a given constitutive relationship for the mass flux, j. The statistical rate theory [32] predicts directly the mass flux in the studied system without the assumption of quasi-equilibrium made in the non-equilibrium thermodynamics. Based on the complete expressions for the liquid evaporation and condensation fluxes, the following second-order approximation is derived [54]

$$j = \sqrt{\frac{2M}{\pi R T_{\mathrm{L}0}}}\, p_{\mathrm{sat}}(T_{\mathrm{L}0}) \left[\frac{p_{\mathrm{sat}}(T_{\mathrm{L}0})}{p_{\mathrm{V}0}} - 1 \right]. \tag{9}$$

Here M is the molar mass of the circumstance, R is the universal gas constant, $p_{\mathrm{sat}}(T_{\mathrm{L}0})$ is the saturation pressure calculated at liquid temperature $T_{\mathrm{L}0}$, and $p_{\mathrm{V}0}$ is the vapor pressure at the interface. Experimental data for steady-state water evaporation/condensation [31, 32, 34, 36] are summarized in Table 1 (the errors of measurements of the evaporation mass flux and vapor pressure for experiments from E5 to

Table 1: Experimental data for steady-state water evaporation/condensation: C1–C4 [34]; E1–E4 [34]; E5–E9 [32]; E10–E24 [31]; E25–E33 [36]

	j, g/(m^{2}s)	p_{V0}, Pa	T_{L0}, °C	T_{V0}, °C
C1	-0.315±0.003	3181±127	25.6±0.05	26.0±0.05
C2	-0.177±0.003	2161±86	19.2±0.05	19.5±0.05
C3	-0.150±0.004	1463±45	12.6±0.05	13.0±0.05
C4	-0.040±0.010	959±32	6.9±0.06	7.5±0.06
E1	1.017±0.013	593±34	-0.4±0.05	2.6±0.05
E2	0.797±0.006	639±34	-0.1±0.05	2.8±0.05
E3	0.595±0.005	616±34	-0.2±0.05	2.4±0.05
E4	0.419±0.005	629±34	-0.1±0.10	2.5±0.10
E5	0.038	1030	9.3±0.1	13.4±0.1
E6	0.068	773	3.7±0.1	8.5±0.1
E7	0.119	546	1.9±0.1	7.3±0.1
E8	0.127	387	-3.8±0.1	4.8±0.1
E9	0.146	293	-9.6±0.1	1.5±0.1
E10	0.2799	596.0	-0.3±0.1	3.2±0.1
E11	0.2544	493.3	-2.9±0.1	0.6±0.1
E12	0.3049	426.6	-4.8±0.1	-0.6±0.1
E13	0.4166	413.3	-5.2±0.1	-1.0±0.1
E14	0.3703	310.6	-8.9±0.1	-3.8±0.1
E15	0.3480	342.6	-7.7±0.2	-2.7±0.1
E16	0.3971	333.3	-7.8±0.1	-1.6±0.2
E17	0.4081	269.3	-10.7±0.1	-4.6±0.1
E18	0.4347	277.3	-10.3±0.1	-4.3±0.2
E19	0.4097	264.0	-11.0±0.2	-4.9±0.1
E20	0.4860	269.3	-10.6±0.1	-4.1±0.1
E21	0.4166	245.3	-11.9±0.1	-6.0±0.1
E22	0.4938	233.3	-12.4±0.1	-5.2±0.1
E23	0.5086	213.3	-13.5±0.1	-6.2±0.1
E24	0.5386	194.7	-14.6±0.1	-6.8±0.4
E25	0.4070±0.006	776.1±12.6	2.73±0.03	4.73±0.02
E26	1.002±0.011	698.8±11.9	1.11±0.02	3.37±0.02
E27	1.371±0.015	599.0±9.9	0.53±0.03	1.84±0.05
E28	1.788±0.018	499.7±8.5	-2.82±0.03	-0.20±0.05
E29	2.544±0.025	397.9±6.8	-6.04±0.03	-2.65±0.05
E30	3.378±0.031	299.7±7.1	-9.67±0.03	-5.66±0.02
E31	3.026±0.028	271.3±5.1	-11.61±0.03	-7.19±0.04
E32	4.242±0.039	268.4±5.3	-12.06±0.04	-7.59±0.06
E33	3.421±0.032	247.5±4.5	-11.86±0.03	-7.31±0.08

E24 are not given in the literature). It is easy to check that the saturation pressure $p_{\rm sat}(T_{\rm L0})$ does not deviate considerably from the measured vapor pressure $p_{\rm V0}$, i.e. the parameter $p_{\rm sat}(T_{\rm L0})/p_{\rm V0} - 1$ is small. Note that the constitutive expression (9) is different than the Hertz-Knudsen [27] formula for the mass flux, j.

Experimental studies of the conditions at the interface during evaporation and condensation [30–36] reported results that are contrary to what generally assumed. These results indicate a temperature discontinuity at the interface in which the temperature in the vapor $T_{\rm V0}$ is greater than that in the liquid $T_{\rm L0}$ by as much as several degrees (see Table 1). Therefore, the classical assumption ($T_{\rm V0} = T_{\rm L0}$) is not fulfilled and an additional relationship between $T_{\rm V0}$ and $T_{\rm L0}$ is needed. Note that the temperature T_{V0} does not appear in the asymptotic expression (9) and the problem of the calculation of temperature discontinuity can be avoided when the stability problem is considered.

3 Stability Analysis of Liquid-Vapor Interface at Steady-State Evaporating (Condensing) Semi-Infinite Layer

Under the experimental conditions [30–36], the steady-state temperature in the liquid phase, $T_{\rm L}(z)$, is a linear function of the vertical coordinate z (Fig. 2). The corresponding temperature distribution in the vapor phase, $T_{\rm V}(z)$, is a complex function of z, see the measured vapor temperature profiles in [30–34, 36]. Because of the low thermal conductivity of the vapor phase and the constant mass flux, j, the temperature gradient is determined from the enthalpy difference between the vapor and liquid

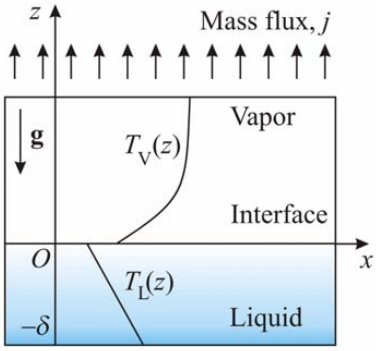

Fig. 2: Sketch of the system under consideration in the case of evaporation. The typical steady-state temperature distribution in the liquid phase, $T_{\rm L}(z)$, and in the vapor phase, $T_{\rm V}(z)$, are illustrated. In the Cartesian coordinate system, *Oxz*, the position of the planar liquid-vapor interface is $z = 0$ and the position of lower boundary is $z = -\delta$.

phases ($h \equiv h_{\rm V} - h_{\rm L}$) and the thermal conductivity of the liquid, $\kappa_{\rm L}$, see (8)

$$\frac{{\rm d}T_{\rm L}}{{\rm d}z} = -\frac{hj}{\kappa_{\rm L}}\,. \tag{10}$$

The position of the Cartesian coordinate system Oxz is illustrated in Fig. 2. The liquid phase is assumed to be semi-infinite with planar interface $z = 0$ and position of the lower boundary $z = -\delta$. In order to follow the common definitions of dimensionless numbers [7–16], the temperature gradient, $\beta \equiv -{\rm d}T_{\rm L}/{\rm d}z$, and the thickness of the liquid layer, δ, are taken as characteristic measures.

In the experiments [30–36], fluctuations of the interfacial shape were not observed. In contrast, when the evaporation flux increases, considerable fluctuations in the interfacial liquid temperature and in the liquid velocity at the surface are measured [36]. For that reason, one simplifies the stability analysis by assuming a *planar* liquid-vapor interface. In this approximation, the equations for the liquid phase can be separated from the respective problem for the vapor phase.

The fluctuations in the temperature, pressure, velocity x- and z-components in the liquid phase are denoted as T_p, p_p, u_p and w_p, respectively. Dimensionless quantities are defined using the following scales [10]: δ for length; $\delta^2\rho_{\rm L}c_{\rm L}^v/\kappa_{\rm L}$ for time; $\kappa_{\rm L}/(\delta\rho_{\rm L}c_{\rm L}^v)$ for velocity; $\eta_{\rm L}^{\rm sh}\kappa_{\rm L}/(\delta^2\rho_{\rm L}c_{\rm L}^v)$ for pressure; $\delta\beta$ for temperature. The dimensionless time and coordinates x and z are τ, ξ and ζ, respectively. In the case of linear stability analysis, the fluctuations can be presented as a superposition of modes with growth rate ω and horizontal wave number k. All functions for fluctuations are proportional to $\exp(\omega\tau + ik\xi)$, where i is the imaginary unit. All amplitudes depend on the vertical coordinate, ζ. In the framework of the Boussinesq approximation, the amplitude of the horizontal velocity component is determined from the continuity equation ($\nabla \cdot \mathbf{v}_{\rm p} = 0$). Therefore, the solution of the problem for the liquid bulk phase is presented as

$$\begin{aligned}(T_{\rm p}, p_{\rm p}) &= \left(\beta\delta A_T, \frac{\eta_{\rm L}^{\rm sh}\kappa_{\rm L}}{\rho_{\rm L}c_{\rm L}^v\delta^2}A_p\right)\exp(\omega\tau + ik\xi)\\ (u_{\rm p}\,, w_{\rm p}) &= \left(\frac{i}{k}\frac{\kappa_{\rm L}}{\rho_{\rm L}c_{\rm L}^v\delta}\frac{{\rm d}A_w}{{\rm d}\zeta}\,, \frac{\kappa_{\rm L}}{\rho_{\rm L}c_{\rm L}^v\delta}A_w\right)\exp(\omega\tau + ik\xi)\end{aligned}\,. \tag{11}$$

The modes with ${\rm Re}(\omega) > 0$ growth with time and those with ${\rm Re}(\omega) < 0$ are stable. The stability limit is defined as follows: ${\rm Re}(\omega) = 0$.

The Reynolds ($N_{\rm Re}$), Rayleigh ($N_{\rm Ra}$), and Prandtl ($N_{\rm Pr}$) numbers characterize the appearing dimensionless groups in the considered problem. These numbers are introduced using the following definitions [10]:

$$N_{\rm Re} \equiv \frac{j\delta}{\eta_{\rm L}^{\rm sh}}\,, \qquad N_{\rm Ra} \equiv -\frac{\rho_{\rm L}\beta g c_{\rm L}^v\delta^4}{\eta_{\rm L}\kappa_{\rm L}}\left(\frac{\partial\rho_{\rm L}}{\partial T_{\rm L}}\right) \qquad N_{\rm Pr} \equiv \frac{\eta_{\rm L}^{\rm sh}c_{\rm L}^v}{\kappa_{\rm L}}\,. \tag{12}$$

After the substitution of the functional form (11) into the momentum and energy balance equations and subsequent linearization of the obtained result, one derives the following system of ordinary differential equations for the amplitudes

$$\frac{\mathrm{d}^3 A_w}{\mathrm{d}\zeta^3} - N_{\mathrm{Re}}\frac{\mathrm{d}^2 A_w}{\mathrm{d}\zeta^2} - (\frac{\omega}{N_{\mathrm{Pr}}} + k^2)\frac{\mathrm{d}A_w}{\mathrm{d}\zeta} - k^2 A_p = 0\,, \tag{13}$$

$$\frac{\mathrm{d}^2 A_w}{\mathrm{d}\zeta^2} - N_{\mathrm{Re}}\frac{\mathrm{d}A_w}{\mathrm{d}\zeta} - (\frac{\omega}{N_{\mathrm{Pr}}} + k^2)A_w - \frac{\mathrm{d}A_p}{\mathrm{d}\zeta} + N_{\mathrm{Ra}}A_T = 0\,, \tag{14}$$

$$\frac{\mathrm{d}^2 A_T}{\mathrm{d}\zeta^2} - N_{\mathrm{Pr}}N_{\mathrm{Re}}\frac{\mathrm{d}A_T}{\mathrm{d}\zeta} - (\omega + k^2)A_T + A_w = 0\,. \tag{15}$$

The magnitude of the convective fluxes due to the vertical mass flow is estimated by the Reynolds number ($N_{\mathrm{Re}} > 0$ for evaporation and $N_{\mathrm{Re}} < 0$ for condensation). The buoyancy effect is accounted for in the momentum balance equations and it is measured with Rayleigh number N_{Ra}. Note that N_{Ra} is negative when the lighter liquid is above the heavier liquid. The ratio between the kinematic viscosity and the thermal diffusivity is given by the Prandtl number, N_{Pr}.

To find the characteristic vertical wave numbers, the amplitudes in equations (13)–(15) are substituted to be proportional to $\exp(n\zeta)$. The condition for the existence of non-trivial solutions (the determinant of the matrix before the respective vector of coefficients to be zero) leads to the following algebraic equation for the dimensionless vertical wave number n:

$$(n^2 - k^2)(n^2 - k^2 - f)(n^2 - k^2 - \frac{f}{N_{\mathrm{Pr}}}) + N_{\mathrm{Ra}}k^2 = 0\,, \tag{16}$$

where the dimensionless Doppler frequency is denoted by $f \equiv \omega + N_{\mathrm{Re}}N_{\mathrm{Pr}}n$. Note that the pure surface modes are located close to the interface and they vanish at infinity – for these modes $\mathrm{Re}(n) \gg 0$. The modes with $\mathrm{Re}(n) \ll 0$ are located close to the lower boundary and if $\mathrm{Re}(n) \approx 1$, the fluctuations appear in a whole liquid layer. For given values of the growth rate and horizontal wave number, equation (16) has six solutions for n: n_m $(m = 1, 2, \ldots, 6)$. The dimensionless Doppler frequency corresponding to n_m is denoted as f_m $(m = 1, 2, \ldots, 6)$. Therefore, the general solution of linear problem (13)–(15) is a superposition of the respective characteristic functions with unknown constants X_m $(m = 1, 2, \ldots, 6)$:

$$A_w = -\sum_{m=1}^{6} (n_m^2 - k^2 - f_m)X_m \exp(n_m\zeta)\,, \tag{17}$$

$$A_p = -\sum_{m=1}^{6} \frac{n_m}{k^2}(n_m^2 - k^2 - \frac{f_m}{N_{\mathrm{Pr}}})(n_m^2 - k^2 - f_m)X_m \exp(n_m\zeta)\,, \tag{18}$$

$$A_T = \sum_{m=1}^{6} X_m \exp(n_m\zeta)\,. \tag{19}$$

Constants X_m ($m = 1, 2, \ldots, 6$) and the dispersion relationship are derived from the mass, momentum, and energy balance boundary conditions at the liquid-vapor interface and at the lower boundary.

The viscous friction from the vapor at the liquid-vapor interface is negligible compared with the viscous friction from the liquid because of the much lower dynamic viscosity of vapor. The surface tension, σ, depends on the liquid temperature and the Marangoni effect must be taken into account in the momentum balance at the interface. Hence the linear form of the tangential stress boundary condition for surface excess linear momentum (7) is simplified [8, 10, 15, 16]

$$\eta_{\mathrm{L}}^{\mathrm{sh}}\left(\frac{\partial u_{\mathrm{p}}}{\partial z}+\frac{\partial w_{\mathrm{p}}}{\partial x}\right)=\left(\frac{\partial \sigma}{\partial T_{\mathrm{L0}}}\right)\frac{\partial T_{\mathrm{p}}}{\partial x} \quad \text{at } z=0\,. \tag{20}$$

If the definitions (11) are substituted into (20), then the following relationship is derived:

$$\frac{\mathrm{d}^2 A_w}{\mathrm{d}\zeta^2}+k^2 A_w+N_{\mathrm{Ma}}k^2 A_T=0 \quad \text{at } \zeta=0\,. \tag{21}$$

Here the expression for the Marangoni number, N_{Ma}, reads

$$N_{\mathrm{Ma}}\equiv-\frac{\beta\rho_{\mathrm{L}}c_{\mathrm{L}}^{v}\delta^2}{\eta_{\mathrm{L}}^{\mathrm{sh}}\kappa_{\mathrm{L}}}\left(\frac{\partial \sigma}{\partial T_{\mathrm{L0}}}\right). \tag{22}$$

Typically $\partial\sigma/\partial T_{\mathrm{L0}} < 0$ and N_{Ma} is positive in the case of evaporation and it is negative for condensation. From general solutions (17) and (19), the boundary condition (21) is reduced to

$$\sum\nolimits_{m=1}^{6}\left[(n_m^2+k^2)(n_m^2-k^2-f_m)-N_{\mathrm{Ma}}k^2\right]X_m=0\,. \tag{23}$$

The fluctuation in the mass flux across the liquid-vapor interface, j_p, is given by $j_p = \rho_L w_p$ calculated at $z = 0$. The fluctuations in the viscous dissipation of energy and in the heat flux of the vapor phase at the liquid-vapor interface are negligible. Hence the linear form of the energy balance equation (8), written for fluctuations at the surface, becomes [15]

$$-\kappa_{\mathrm{L}}\frac{\partial T_{\mathrm{p}}}{\partial z}=\rho_{\mathrm{L}}hw_{\mathrm{p}}+\frac{3}{2}\left(\frac{j^2}{\rho_{\mathrm{V}}^2}-\frac{j^2}{\rho_{\mathrm{L}}^2}\right)\rho_{\mathrm{L}}w_{\mathrm{p}}+\frac{2\eta_{\mathrm{L}}^{\mathrm{sh}}j}{\rho_{\mathrm{L}}}\frac{\partial w_{\mathrm{p}}}{\partial z} \quad \text{at } z=0\,. \tag{24}$$

The second term in the right-hand side of (24) accounts for the kinetic energy transfer due to the mass flux from one phase to the other. For typical values of parameters for water, $h = 2.5 \times 10^6$ J/kg, $j = 2$ g/(m^{2}s) and $\rho_V = 5.2 \times 10^{-3}$ kg/m^3, this term

becomes six orders of magnitudes smaller than the first term on the right-hand side of (24) and it can be neglected. The third term in the right-hand side of (24) represents the viscous dissipation of energy in the liquid phase. This term will be comparable to $\rho_{\mathrm{L}} h w_p$ if the vertical decay length of the velocity is smaller than $2j\eta_{\mathrm{L}}^{\mathrm{sh}}/(\rho_{\mathrm{L}}^2 h)$. For water density $\rho_{\mathrm{L}} = 9.8\times10^3$ kg/m^3 and dynamic viscosity $\eta_{\mathrm{L}}^{\mathrm{sh}} = 1.6\times10^{-3}$ kg/(ms), the characteristic thickness $2j\eta_{\mathrm{L}}^{\mathrm{sh}}/(\rho_{\mathrm{L}}^2 h)$ becomes unphysically small, 3×10^{-18} m. Therefore, the viscous dissipation of fluctuations can be neglected and the boundary condition (24) in terms of definition (11) is considerably simplified

$$N_{\mathrm{Re}} N_{\mathrm{Pr}} \frac{\mathrm{d}A_T}{\mathrm{d}\zeta} + A_w = 0 \ \text{ at } \ \zeta = 0\,. \tag{25}$$

To close the system of equations, the normal stress boundary condition (7) and the expression for the mass flux (9) are applied. The fluctuation in the vapor pressure $p_{\mathrm{V}p}$ is calculated from the normal stress boundary condition (7) written in its linear form for perturbations [15, 18–26]

$$p_{\mathrm{p}} - 2\eta_{\mathrm{L}}^{\mathrm{sh}} \frac{\partial w_{\mathrm{p}}}{\partial z} - 2\frac{j_{\mathrm{p}} j}{\rho_{\mathrm{V}}} = p_{\mathrm{V}p} \ \text{ at } \ z = 0\,. \tag{26}$$

The second term in the left-hand side of (26) represents the dynamic pressure of the liquid phase – the corresponding dynamic pressure of the vapor phase is much smaller because of the smaller vapor dynamic viscosity. The third term accounts for the momentum transport due to the mass flux across the interface. The vapor density ρ_{V} is six orders of magnitude smaller than the liquid density ρ_{L} and the momentum loss from the liquid is omitted. Following the assumption that the interfacial shape does not change, the capillary pressure in (26) becomes zero.

The leading order with respect to the small parameter $p_{\mathrm{sat}} T_{\mathrm{L}0}/p_{\mathrm{V}0} - 1$ of the statistical rate theory expression for the mass flux (9) gives the following simple relationship for perturbations at interface:

$$j_{\mathrm{p}} = \sqrt{\frac{2M}{\pi R T_{\mathrm{L}0}}} \left[\left(\frac{\partial p_{\mathrm{sat}}}{\partial T_{\mathrm{L}}} \right) T_{\mathrm{p}} - p_{\mathrm{V}p} \right] \ \text{ at } \ z = 0\,. \tag{27}$$

If the pressure, $p_{\mathrm{V}p}$, is eliminated from equations (26) and (27) and the definitions for amplitudes (11) are used, then the missing boundary condition is found to be

$$A_w - N_{\mathrm{Re}} N_{\mathrm{Pr}} N_{\mathrm{Bi}} A_T - N_{\mathrm{Re}} N_{\mathrm{Br}} \left(2\frac{\mathrm{d}A_w}{\mathrm{d}\zeta} - A_p \right) = 0 \ \text{ at } \ \zeta = 0\,. \tag{28}$$

The new dimensionless groups N_{Bi} and N_{Br} appearing in (28) are defined as follows:

$$N_{\mathrm{Bi}} \equiv \frac{\delta \kappa_s}{\kappa_{\mathrm{L}}}\,, \qquad N_{\mathrm{Br}} \equiv \frac{\kappa_s (\eta_{\mathrm{L}}^{\mathrm{sh}})^2}{\rho_{\mathrm{L}} \kappa_{\mathrm{L}} \beta \delta^2} \left(\frac{\partial p_{\mathrm{sat}}}{\partial T_{\mathrm{L}0}} \right)^{-1}, \tag{29a}$$

where parameter κ_s is calculated from the expression

$$\kappa_s \equiv h\left(\frac{\partial p_{\rm sat}}{\partial T_{\rm L0}}\right)\left(\sqrt{\frac{\pi R T_{\rm L0}}{2M}} - \frac{2j}{\rho_{\rm V}}\right)^{-1}. \tag{29b}$$

The explanation of the physical meaning of $N_{\rm Bi}$ and $N_{\rm Br}$ is discussed below.

In the literature, in spite of energy balance equation (8), the Neumann boundary condition for the heat flux is postulated [7, 8, 10, 18–26] – the temperature gradient at the interface is proportional to the temperature difference. The coefficient of proportionality is called the "heat transfer coefficient" and the dimensionless number corresponding to it is called the "Biot number". The experimental data for evaporation and condensation [31–36] do not fit the Neumann boundary condition and they are in agreement with the statistical rate theory expression for the mass flux (9). To obtain a deeper understanding of the meaning of dimensionless numbers $N_{\rm Bi}$ and $N_{\rm Br}$, equation (28) is substituted into (25). The obtained result reads

$$\frac{{\rm d}A_T}{{\rm d}\zeta} + N_{\rm Bi}A_T + \frac{N_{\rm Br}}{N_{\rm Pr}}\left(2\frac{{\rm d}A_w}{{\rm d}\zeta} - A_p\right) = 0 \ \text{ at } \ \zeta = 0\,. \tag{30}$$

If $N_{\rm Br}$ is equal to zero, equation (30) is reduces exactly to equation (6) in ref. [10] applied to the investigation of the stability of a non-evaporating liquid layer heated (cooled) from below (the Nield problem [8]). Expression (29a) for $N_{\rm Bi}$ corresponds exactly to the Biot number defined in [10] and to number L in [8]. The parameter κ_s has the meaning of the heat transfer conductivity – in our case the heat transfer conductivity is strictly defined with respect to the properties of the evaporating (condensing) liquid-vapor interface through (29b). At fixed temperature $T_{\rm L0}$, the heat transfer conductivity is greater for evaporation than that for condensation. Note that for typical liquids in steady-state evaporation (condensation), the mass flux cannot exceed 5 g/(m^{2}s) and practically $N_{\rm Bi}$ is always positive.

If equation (30) is compared with (29a) and (29b) in [15], it can be shown that $N_{\rm Br}$ corresponds to the so-called "Brinkman number", which accounts for the effect of the dynamic pressure fluctuations on the energy transfer between the phases. Here $N_{\rm Br}$ is not a free parameter – it is calculated from the physical properties of the liquid through (29a) and (29b). For typical mass transfer processes, $N_{\rm Br}$ is positive in the case of evaporation and negative for condensation.

If the general solution (17)–(19) are substituted into boundary conditions (25) and (30), the following equations are derived:

$$\sum\nolimits_{m=1}^{6} \left[N_{\rm Re}N_{\rm Pr}n_m - (n_m^2 - k^2 - f_m)\right]X_m = 0\,, \tag{31}$$

$$\sum\nolimits_{m=1}^{6} \left[n_m + N_{\rm Bi} + \frac{N_{\rm Br}}{N_{\rm Pr}}\frac{n_m}{k^2}(n_m^2 - k^2 - f_m)\left(n_m^2 - 3k^2 - \frac{f_m}{N_{\rm Pr}}\right)\right]X_m = 0\,. \tag{32}$$

To close the problem, the boundary conditions at the lower boundary, $\zeta = -1$, are applied. In experiments [31–34, 36], the temperature and the mass flux at lower boundary are strictly controlled. Therefore, the fluctuations of the temperature and velocity at the lower boundary are equal to zero in our stability analysis. From the other viewpoint, these boundary conditions give the possibility of comparing the numerical results in Section 4 with those reported in the literature [8, 10, 14–16]. From the general solution (17)–(19), one derives the following relationships:

$$\sum_{m=1}^{6} (n_m^2 - k^2 - f_m) \exp(-n_m) X_m = 0 \,, \tag{33}$$

$$\sum_{m=1}^{6} n_m (n_m^2 - k^2 - f_m) \exp(-n_m) X_m = 0 \,, \tag{34}$$

$$\sum_{m=1}^{6} \exp(-n_m) X_m = 0 \,. \tag{35}$$

The linear system of equations (23) and (31)–(35) for constant X_m ($m = 1, 2, \ldots, 6$), in which the characteristic vertical wave numbers n_m are solutions of equation (16), has a non-trivial solution when the determinant of the matrix before the vector of coefficients $\mathbf{X}$ is equal to zero. This condition defines the dispersion relationship for the calculation of the growth rate, ω, for a given horizontal wave number, k.

4 Numerical Results and Discussions

There are two ways to describe numerical results. The first is to calculate the stability diagram $\mathrm{Re}(\omega) = 0$ as a function of dimensionless numbers (the Nield diagrams [8, 10]) without taken into account the concrete physical system. This approach is quite general and it is difficult to find the effect of physical parameters (temperature, magnitude and sign of the mass flux, etc.) on the stability of our system. One has six dimensionless numbers and, therefore, the general stability diagrams are five-dimensional. For example, the critical Marangoni number becomes a function of N_{Pr}, N_{Re}, N_{Ra}, N_{Bi}, and N_{Br}.

The second approach is to specify the concrete typical physical system and to calculate the solutions of the dispersion relationship. Then all dimensionless numbers become functions of the temperature at the interface, T_{L0}, the mass flux, j, and the thickness of liquid layer, δ. Moreover, information about the wavelength and wave growth rate is obtained in real physical units and can be analyzed. Below, the pure water phase is chosen and the dimensionless numbers are calculated as a function of T_{L0} from -12 to 25°C.

If the dimensionless numbers of the stability problem are known for a given interfacial liquid temperature, T_{L0}, mass flux, j, and liquid layer thickness, δ, then their values for other mass flux and thickness can be simply calculated. From (12), (22), and (29a), the Reynolds, Rayleigh, and Marangoni numbers are proportional to

the mass flux, while the Brinkman number is inversely proportional to j. The thickness of the liquid layer influences the values of the dimensionless groups as follows: $N_{\mathrm{Re}} \sim \delta$; $N_{\mathrm{Ra}} \sim \delta^4$; $N_{\mathrm{Ma}} \sim \delta^2$; $N_{\mathrm{Bi}} \sim \delta$; $N_{\mathrm{Br}} \sim 1/\delta^2$.

Figure 3 shows the calculated values of N_{Pr}, N_{Re}, N_{Ma}, N_{Ra}, N_{Bi}, and N_{Br} as functions of temperature, T_{L0}, for water at $j = 2$ g/(m^{2}s) and $\delta = 3.5$ mm. The physical properties of water in the temperature interval from 0 to 25°C are taken from [55]. The dependence $p_{\mathrm{sat}}(T_{\mathrm{L0}})$ for liquid-vapor water in the temperature interval -15.8 to 0°C is tabulated in [56]. Other liquid water parameters are extrapolated in the temperature interval -12 to 0°C. The temperature interval from -12 to 25°C is chosen from available experimental data [31–34, 36] for evaporation and condensation of pure water summarized in Table 1.

The Prandtl number has values between 22 and 6 and decreases with temperature (Fig. 3a). The Reynolds number has small values and it increases from 2.6×10^{-3} to 6.7×10^{-3} (Fig. 3a). The Marangoni and Rayleigh numbers have large values (of the order of 10^4) and they increase with temperature (Fig. 3b). Hence the effect of gravity cannot be neglected and both surface tension-driven and buoyancy convection play a role in the stability of a liquid layer. For evaporation, N_{Ra} is negative below 4°C and it is positive for higher temperatures.

The Biot number is one order of magnitude smaller than the Marangoni number and it increases from 750 to 6.6×10^3 when the temperature increases from -12 to 25°C (Fig. 3c). According to the classification of Nield [8], these high values of N_{Bi} correspond to the case of a "conducting interface". Finally, the Brinkman number is very small – it decreases monotonically from 6.8×10^{-4} to 0.95×10^{-4} with increase of T_{L0}.

Note that the formal substitution of $N_{\mathrm{Re}} = 0$ and $N_{\mathrm{Br}} = 0$ in boundary conditions (25) and (30) reduces our problem to the stability problem of non-evaporating/non-condensing liquid layer [7, 8, 10]. The small values of N_{Re} and N_{Br} may lead to the wrong conclusion that the convective terms in the momentum balance equations (13) and (14) and the effect of the dynamic pressure fluctuations on the energy transfer between phases (30) are negligible. As shown below these factors are import for the appearance of interfacial instability modes.

To obtain a deeper understanding of the stability diagrams, typical numerical solutions of the dispersion relationships for dimensionless growth rate $\omega = \omega(k)$ are illustrated and discussed below. The solutions are sorted in such a way that mode "0" corresponds to the solution with the highest $\mathrm{Re}(\omega)$, mode "1" to the next solution with smaller $\mathrm{Re}(\omega)$, etc.

It is important to note that mode 0 exists for all cases under consideration (evaporation and condensation in the studied interval of temperatures). The wave growth rate has only a real part with very high values (Fig. 4), i.e. the system is unstable and

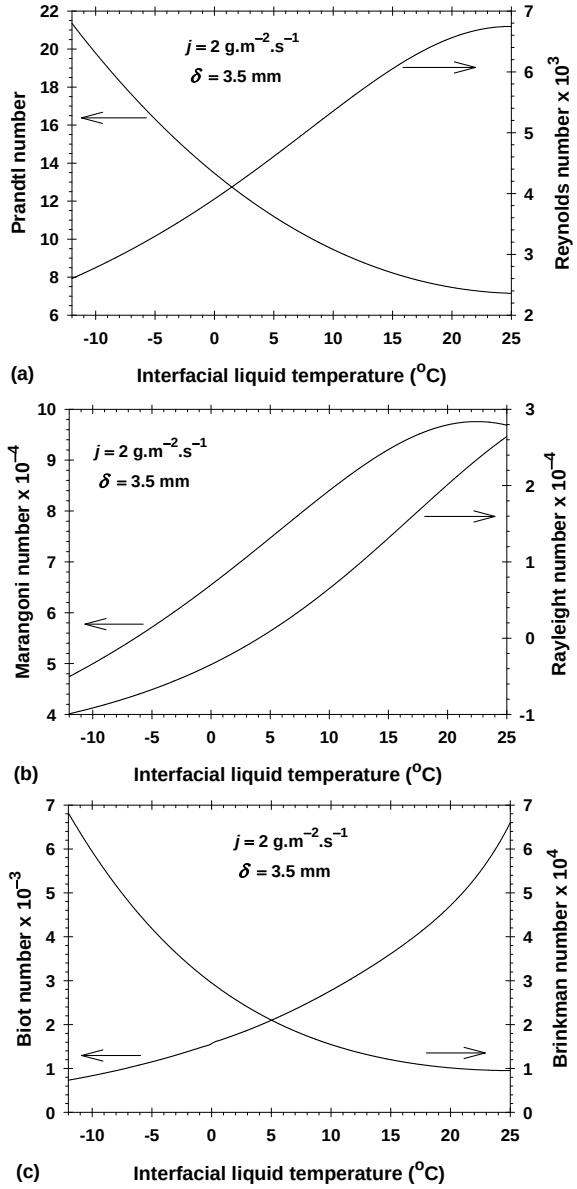

Fig. 3: Dimensionless numbers as functions of liquid interfacial temperature $T_{\mathrm{L}0}$ for water at fixed evaporation flux 2 g/(m^{2}s) and thickness of the liquid layer 3.5 mm: (a) N_{Pr} and N_{Re}; (b) N_{Ma} and N_{Ra}; (c) N_{Bi} and N_{Br}.

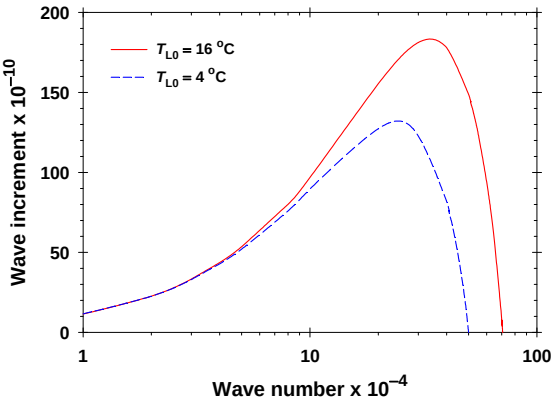

Fig. 4: Dimensionless wave increment Re(ω) vs dimensionless horizontal wave number k for mode 0. The evaporation mass flux is 4 g/(m^{2}s), $\delta = 3.5$ mm, and $T_{\rm L0} = 16$ and 4°C.

the modes develop very fast. If the sign of the mass flux changes from evaporation to condensation, then the wave increment changes by not more than 1%. Therefore, the direction of the mass flux does not influence considerably the stability diagrams. The difference between two curves in Fig. 4 calculated at $T_{\rm L0} = 16$ and 4°C does not occur because of significantly different values of the Rayleigh number. The main factors which control the process are the Reynolds, Brinkman, and Biot numbers, i.e. the convective fluxes and the interfacial momentum loss. The dimensionless wave numbers are also very high – the wavelengths are small. The corresponding vertical decay numbers are proportional to $\omega^{1/2}$ and the instability modes are located close to the interface. We will call these modes "interfacial instability modes". The following conclusion can be drawn: the dilatational (longitudinal) surface waves described by equation (23) in [10] cannot appear at evaporation/condensation interfaces – the mechanism of instability has a different physical explanation.

Other wave modes (1, 2, ..., 6) do not have such high values of the dimensionless wave growth rate. Their physical behavior is similar to those for the non-evaporating/non-condensing case [10]. For evaporation mass flux 2 g/(m^{2}s), $\delta = 3.5$ mm and $T_{\rm L0} = 16$°C (Fig. 5a), modes 1 and 2 have positive values of Re(ω) for wave numbers between 0.45 and 10.4 (mode 1) and 3.2 and 7.2 (mode 2). These two modes are unstable in the respective wave number intervals. The modes with wave numbers below 0.45 and 10.4 are stable. All modes (1–6) have only real parts and only stable modes 5 and 6 have a small interval of wave numbers from 1.4 to 1.55 where the dimensionless frequency achieves a maximum of 4.71 (Fig. 5a). If the temperature decreases to $T_{\rm L0} = 4$°C (Fig. 5b), where the buoyancy force be-

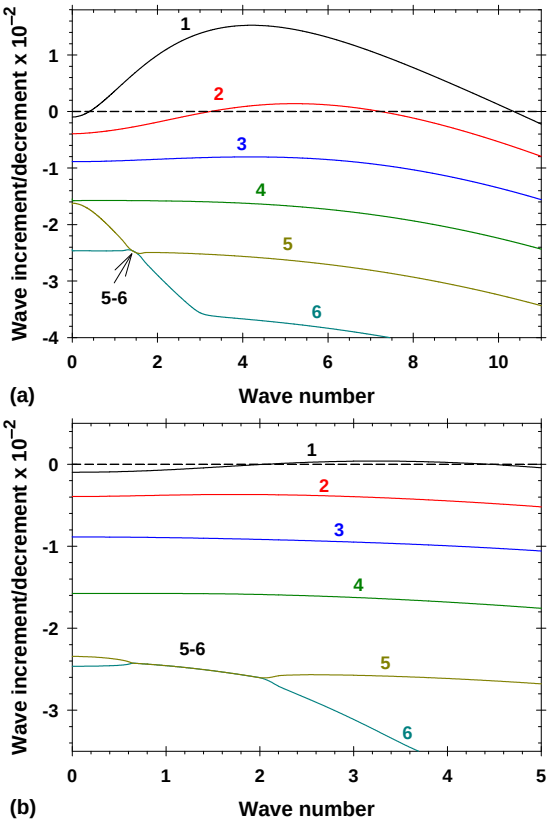

Fig. 5: Dimensionless wave increment/decrement Re(ω) vs dimensionless horizontal wave number k for modes 1-6: (a) $T_{\mathrm{L0}} = 16°\mathrm{C}$; (b) $T_{\mathrm{L0}} = 4°\mathrm{C}$ (negligible buoyancy effect). The evaporation mass flux is 2 g/(m^{2}s) and $\delta = 3.5$ mm.

comes negligible, the system becomes more stable – the main destabilizing factor is the Marangoni force. Mode 2 does not have an instability interval of the wave numbers and the corresponding interval for mode 1 becomes considerably narrow from $k = 2.1$ to $k = 4.4$. The region where modes 5 and 6 have an imaginary part (from $k = 0.65$ to $k = 2.05$) is wider. The corresponding maximum of the dimensionless frequency in this interval is higher and equals to 8.73.

Therefore, the lower the temperature is the more stable is the system. For a whole range of temperatures unstable modes with imaginary parts are not found. The oscillatory instability regime found in [10] does not take place for studied values of the physical parameters.

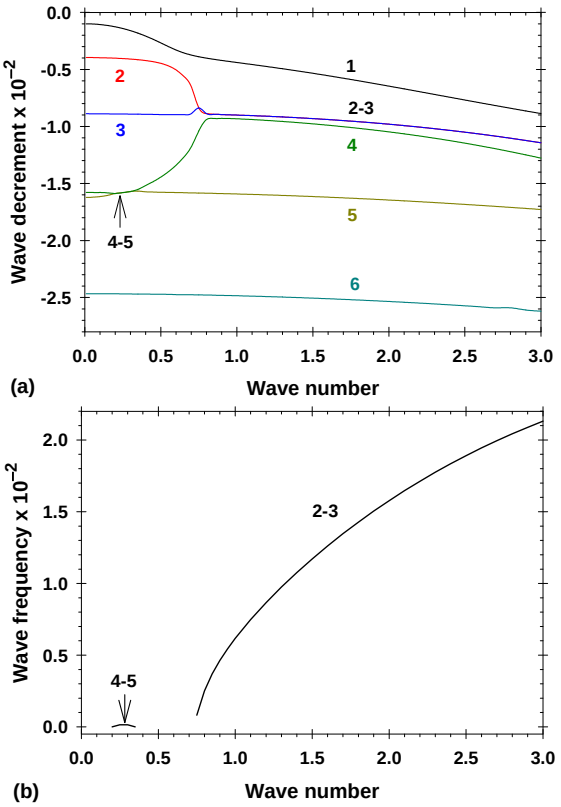

Fig. 6: Solutions of the dispersion relationship for condensation flux 2 g/(m^{2}s) and $\delta = 3.5$ mm: (a) dimensionless wave decrement vs k for modes 1-6; (b) dimensionless frequency vs k for modes 2-3 and 4-5.

In contrast, in the case of condensation flux -2 g/(m^{2}s), $\delta = 3.5$ mm and $T_{\mathrm{L0}} = 16°$C (Fig. 6a), all modes 1–6 are stable. The wave decrements have the same order of magnitude as in Fig. 5a. The number of stable oscillatory modes increases: modes 2 and 3 for wave numbers greater than 0.73; modes 4 and 5 for k from 0.20 to 0.37. The corresponding frequencies of modes 2 and 3 increase monotonically while those for modes 4 and 5 have small values (Fig. 6b). The numerical results for modes 1–6 (Figs. 5 and 6) confirm qualitatively the Neild diagram [8] – the stability of the system is determined mainly by the signs of the Marangoni and Rayleigh numbers and do not depend considerably on the direction of mass flux j. It is very important to note that modes 1–6 have moderate values of n and, therefore, the fluctuations are developed in the whole liquid layer.

We showed that the oscillatory instability regime does not occur for the investigated system – the stability limit is calculated from the equation $\omega(k_{\rm cr}) = 0$ for modes 0, 1, and eventually 2 where it appears. To have a better physical feeling for the numbers in the graphs below, the critical wavelength, $\lambda_{\rm cr} \equiv \pi\delta/k_{\rm cr}$, is used. We found a simple asymptotic solution for the critical wave number of mode 0 (see Appendix)

$$k_{\rm cr} = \frac{1}{2N_{\rm Re}N_{\rm Br}} + N_{\rm Bi}\,. \tag{36a}$$

For all investigated cases, the heat transfer conductivity, κ_s, has a week dependence on the mass flux, j, see (29b). Therefore, the Biot number $N_{\rm Bi}$ and the parameter $N_{\rm Re}N_{\rm Br}$ appearing in (36a) do not depend considerably on j, see (12) and (29a). Equation (36a) can be rewritten in physical parameters for the critical wavelength of mode 0 using definitions (12) and (29a)

$$\lambda_{\rm cr} = \pi\left[\frac{\kappa_s}{\kappa_{\rm L}} + \frac{\rho_{\rm L}h}{2\kappa_s\eta_{\rm L}^{\rm sh}}\left(\frac{\partial p_{\rm sat}}{\partial T_{\rm L0}}\right)\right]^{-1}. \tag{36b}$$

As can be expected, λ_{cr} does not depend on the thickness of liquid layer δ and the relationship (36b) has a universal form – it depends only on the physical properties of the system but not on the geometrical parameters.

The numerical results for the critical wavelength at two high mass fluxes, -10 and 10 g/(m^{2}s), are shown in Fig. 7. The difference between the two curves is small – it arises only because of the weak dependence of $\lambda_{\rm cr}$ on the mass flux, j. In the case

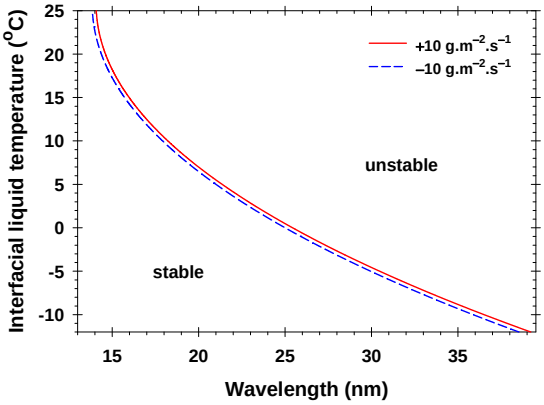

Fig. 7: Stability diagram for interfacial wave mode 0 at two large mass fluxes, $j = -10$ and 10 g/(m^{2}s).

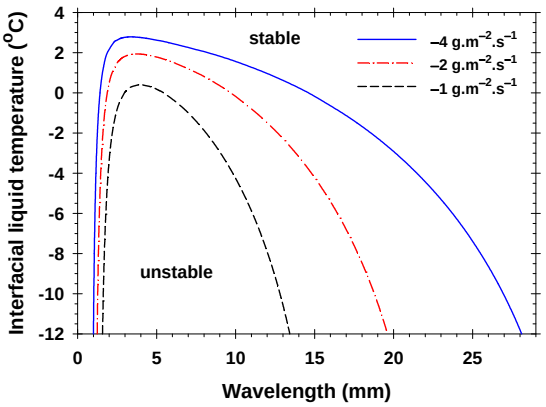

Fig. 8: Stability diagram for mode 1, $\delta = 3.5$ mm and different condensation fluxes: -4, -2 and -1 g/(m^{2}s). All other modes are stable.

of condensation, the heat transfer coefficient, κ_s, is smaller than that for evaporation with other physical parameters fixed, see (29b). The critical wavelengths are of the order of nanometers and they decreases with the increase in temperature (Fig. 7). The respective fluctuations vanish at infinity as $\exp(k_{\rm cr}\zeta)$ and, therefore, they are located close to the interface (see Appendix). This is the reason for the inset of interfacial turbulence at an evaporating/condensing liquid-vapor interface. Other unstable modes appear in the bulk phase – they have considerably larger vertical decay lengths.

In the case of condensation, the stability diagrams for mode 1 and three mass fluxes are illustrated in Fig. 8. The larger the mass flux is, the wider is the region of unstable fluctuations. The modes 2, 3, ... are stable. The critical wavelengths are of the order of millimeters and the curves are not symmetric with respect to a given wave number (Fig. 8). In the area of shorter waves, curves $T_{\rm L0} = T_{\rm L0}(k_{\rm cr})$ are closer each to the other. Note that the Marangoni number is negative for condensation ($N_{\rm Ma} < 0$) and the surface forces stabilize the fluctuation. When the temperature is below 4°C the Rayleigh number is positive ($N_{\rm Ra} > 0$) and the gravity force destabilizes the convection flow in the bulk. For a given temperature, the thermal expansion coefficient of water becomes large enough for the buoyancy convection to reverse the fluctuations from stable Marangoni type to unstable Rayleigh type. When the Rayleigh number is negative, both surface and gravity forces stabilize the fluctuations and, therefore, for temperatures higher than 4°C and condensations all modes 1, 2, ... are stable. This conclusion is in qualitative agreement with the Nield diagram [8].

In the case of evaporation, modes 1 and 2 can have positive Re(ω) and all other modes are stable. For evaporation, the Marangoni number is positive ($N_{\rm Ma} > 0$) and the gradient of surface tension gives rise of fluctuations at the interface. The curves

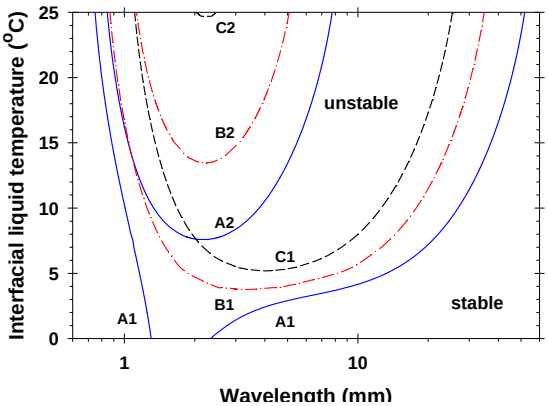

Fig. 9: Stability curves for mode 1 (curves A1, B1 and C1) and mode 2 (curves A2, B2 and C2). The thickness of liquid layer is $\delta = 3.5$ mm. The evaporation fluxes corresponding to A, B, and C are 4, 2, and 1 g/(m^{2}s), respectively. All other modes are stable.

$T_{\rm L0} = T_{\rm L0}(k_{\rm cr})$ for three evaporation fluxes, 4 (curves A), 2 (curves B) and 1 g/(m^{2}s) (curves C) are plotted in Fig. 9. The temperature interval is from 0 to 25°C. The larger the evaporation fluxes are, the more unstable are the systems. The asymmetry of the stability curves with respect to the wave number is well pronounced. Below 4°C, the Rayleigh number has negative values (see Fig. 3b) but the gravity force is not strong enough to suppress the wave growth. Especially for evaporation flux 4 g/(m^{2}s) curves A1 make an open area of unstable modes up to 0°C, which continues below 0°C (compare Figs. 9 and 10).

The stability diagrams $T_{\rm L0} = T_{\rm L0}(k_{\rm cr})$ for three evaporation fluxes, 4, 3.5, and 3 g/(m^{2}s), are plotted in Fig. 10 for temperatures below 0°C where the Marangoni number is positive (favoring wave growth) and the Rayleigh number is negative (suppressing corrugation development). These points belong to the narrow region $N_{\rm Ma} > 0$ and $N_{\rm Ra} < 0$ of the Nield diagram where the locus bounds a much smaller area. When the evaporation flux is below 3 g/(m^{2}s), the unstable modes do not appear (Fig. 10). These calculations are in good agreement with experimental observations [36].

In the experiments given in Table 1, the following interesting phenomena were observed. First, in all experiments a uniform-temperature layer immediately below the interface in the liquid is measured. The thickness of this layer is very small (of the order of micrometers) and it decreases when the mass flux increases. The fluctuations in the temperature of liquid close to the interface were also measured [36]. The amplitudes of fluctuations are small (about 0.1 K) and the power spectrum of fluctuations

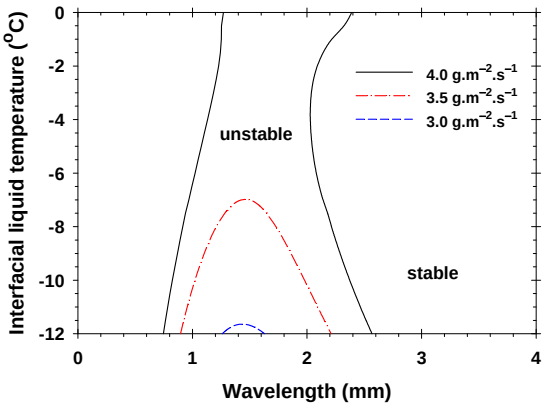

Fig. 10: Stability diagram for mode 1, evaporation fluxes 4, 3.5, and 3 g/(m^{2}s) and $\delta = 3.5$ mm. The temperature interval corresponds to a stabilizing effect of the buoyancy force.

has no a favored frequency – all frequencies have approximately the same probability. This observation is in a good agreement with the interfacial instability modes, see Figs. 4 and 7. The direction of the mass flux (evaporation and condensation) does not change the stability diagram significantly. Owing to the intensive growth of interfacial modes, they interact with each other and form a layer with an intensive mixture of modes – measured as a uniform temperature layer. The interfacial modes decay very fast in depth from the interface and, therefore, the uniform temperature layer is stable overall and stays at the interface. The second phenomenon is listed in Table 1 – in all experiments E25–E33 the temperature at the lower boundary was fixed 3.5°C. Therefore, when the vapor pressure decreases, the evaporation flux j must increase. Note that in all experiments the buoyancy force acts as a stabilizing factor – the lighter liquid is above the heavier. Nevertheless, when the vapor pressure is lower than 299.7 Pa (see E30 in Table 1), the expected trend of the evaporation flux was not measured. At 299.7 Pa the measured evaporation flux was 3.378 g/(m^{2}s). If this observation is compared with the stability diagram (Fig. 10), it is well illustrated that at the corresponding temperatures and mass fluxes, the flow becomes unstable not only at the interface but also in the whole liquid bulk phase. Marangoni-type instability takes place. This may be the reason for the change of regime in experiments E31–E33. Note that all measured parameters indicate the transition to turbulence located not only close to the interface: the surface velocity and the amplitudes of fluctuations in the temperature and velocity increase rapidly [36].

5 CONCLUSIONS

The stability of a liquid layer of pure substances under a steady-state evaporation/condensation has been described. The general mass, momentum and energy balance equations in the bulk and at the liquid-vapor interface were applied. To close the problem, the statistical rate theory expression for the mass flux across the interface was used in its simpler form. It is pointed that the problem is unclosed because of missing boundary conditions for the measured temperature jump at interface. In the case of a linear stability analysis of the liquid-vapor interface, this problem can be avoided by assuming a non-deformable interface. The respective system of equations in the bulk and at the interface was solved and the dispersion relationship for the wave growth rate and wavelengths was derived.

From numerical results in Section 4 obtained for pure water in the temperature interval from -12 to 25°C, the following conclusions can be drawn. The oscillatory instability regime does not take place for the investigated system – all unstable modes have only a fluctuation increment. In spite of the direction of mass flux (condensation and evaporation), interfacial instability modes appear. They grow very fast but their decay lengths from the interface are very small (of the order of several nanometers). The critical wavelength is small (from 15 to 40 nm) and the stability region becomes wider with decrease in temperature (see Fig. 7). Other possible instability modes have millimeter-sized vertical wave numbers – they are developed in the bulk phase. The reasons for bulk instability are the buoyancy force (when the lighter liquid is above the heavier) or the Marangoni force arising from the lateral fluctuations in surface tension because of fluctuations in temperature. Qualitative agreement of these modes with the Nield diagram [8] is found – the values are different because of the effect of bulk convection forces, surface momentum loss due to the mass flux, etc. (different boundary conditions are used).

The present stability analysis shows good agreement with experiments [31, 32, 34, 36]. Nevertheless, some open questions arise. When the temperature changes considerably in the liquid layer, is the Boussinesq approach valid? What are the errors arising from the assumptions of linear dependence of the density on temperature? How do the instability modes interact in order to form an almost uniform temperature layer as observed experimentally and what is the mechanism of the energy transport in the constant-temperature layer? The author is convinced that the main answers to these questions can be found by applying non-linear analysis based on the general physical transport equations.

ACKNOWLEDGEMENTS

The author is grateful to Project CoE "National center of mechatronics and clean technologies" BG05M2OP001-1.001-0008 of the Operational Programme "Science and Education for Smart Growth 2014–2020".

APPENDIX: CRITICAL WAVE NUMBER FOR INTERFACIAL MODES

The numerical results in Section 4 show that the critical wave number $k_{\rm cr}$ of interfacial modes is very high, of the order of 10^5 (see Fig. 4). The instability waves have no oscillatory part and the stability limit is defined with $\omega(k_{\rm cr}) = 0$. In this case, the characteristic equation (16) has a triple solution, $n \approx k_{\rm cr}$. Therefore, the vertical decay length is very small and we will look for a solution that is located close to the interface. The approximate solution with precision $N_{\rm Re}N_{\rm Pr}/k_{\rm cr}$ of the system (13)–(15) is

$$A_p = X_p \exp(k_{\rm cr}\zeta)\,, \tag{A3}$$

$$A_w = (X_w + \frac{X_p}{2}\zeta)\exp(k_{\rm cr}\zeta)\,, \tag{A4}$$

$$A_T = [X_T - \frac{X_w}{2k_{\rm cr}}\zeta + \frac{X_p}{8k_{\rm cr}^2}(\zeta - k_{\rm cr}\zeta^2)]\exp(k_{\rm cr}\zeta)\,, \tag{A5}$$

where the unknown constants X_p, X_w, and X_T are calculated from the boundary conditions at the interface.

If expressions (A3)–(A5) are substituted into the tangential stress boundary condition (21), then the amplitude of pressure fluctuations is derived

$$X_p = -2k_{\rm cr}X_w - N_{\rm Ma}k_{\rm cr}X_T\,. \tag{A6}$$

The solutions (A3)–(A6) are used to calculate the relationship between the amplitudes of velocity and temperature from boundary condition (25)

$$X_w + N_{\rm Re}N_{\rm Pr}k_{\rm cr}(1 - \frac{N_{\rm Ma}}{k_{\rm cr}^2})X_T = 0\,. \tag{A7}$$

The normal stress boundary condition (28) yields

$$(1 - 2N_{\rm Re}N_{\rm Br}k_{\rm cr})X_w - N_{\rm Re}N_{\rm Pr}N_{\rm Bi}X_T = 0\,. \tag{A8}$$

The homogeneous system of equations (A7) and (A8) has a solution, if the normalized critical wave number $\tilde{k}_{\rm cr} \equiv 2N_{\rm Re}N_{\rm Br}k_{\rm cr}$ becomes a solution of the following cubic equation:

$$(1 - \tilde{k}_{\rm cr})(2\tilde{k}_{\rm cr}^2 - N_{\rm Ma}N_{\rm Re}^2N_{\rm Br}^2) + 4N_{\rm Re}N_{\rm Br}N_{\rm Bi}\tilde{k}_{\rm cr} = 0\,. \tag{A9}$$

For the investigated temperature interval (see Fig. 3), the values of $N_{\mathrm{Ma}}N_{\mathrm{Re}}^2N_{\mathrm{Br}}^2$ and $N_{\mathrm{Re}}N_{\mathrm{Br}}N_{\mathrm{Bi}}$ are very small. Therefore, the approximate solution of equation (A9) is

$$\tilde{k}_{\mathrm{cr}} = 1 + 2N_{\mathrm{Re}}N_{\mathrm{Br}}N_{\mathrm{Bi}}\,. \tag{A10}$$

The relative precision of approximate solution (A10) for all studied temperatures and an absolute value of the mass flux smaller than 5 g/(m^{2}s) is better than 0.1%.

References

[1] H. Bénard (1901) Les Tourbillons Cellulaires dans une Nappe Liquide Transportant de la Chaleur par Convection en Régime Permanent. *Annales de Chimie et de Physique* **23** 62-144.

[2] J.W.S. Rayleigh (Lord) (1916) On convective currents in a horizontal layer of fluid when the higher temperature is on the underside. *Philosophical Magazine* **32** 529-546.

[3] H. Jeffreys (1926) The stability of a layer of fluid heated below. *Philosophical Magazine* **2** 833-844.

[4] H. Jeffreys (1928) Some cases of instability in fluid motion. *Proceedings of the Royal Society A* **118** 195-208.

[5] A.R. Low (1929) On the criterion for stability of a layer of viscous fluid heated from below. *Proceedings of the Royal Society A* **125** 180-195.

[6] A. Pellew, R.V. Southwell (1940) On maintained convective motion in a fluid heated from below. *Proceedings of the Royal Society A* **176** 312-343.

[7] J.R.A. Pearson (1958) On convection cells induced by surface tension. *Journal of Fluid Mechanics* **4** 489-500.

[8] D.A. Nield (1964) Surface tension and buoyancy effect in cellular convection. *Journal of Fluid Mechanics* **19** 341-352.

[9] C.V. Sternling, L.E. Scriven (1959) Interfacial turbulence: hydrodynamic instability and the Marangoni effect. *AIChE Journal* **5** 514-523.

[10] A.Ye. Rednikov, P. Colinet, M.G. Velarde, J.C. Legros (2000) Rayleigh–Marangoni oscillatory instability in a horizontal liquid layer heated from above: coupling and mode mixing of internal and surface dilational waves. *Journal of Fluid Mechanics* **405** 57-77.

[11] K.C.D. Hickman (1952) Surface Behavior in the Pot Still. *Industrial and Engineering Chemistry* **44** 1892-1902.

[12] K. Hickman (1972) Torpid Phenomena and Pump Oils. *Journal of Vacuum Science & Technology* **9** 960-976.

[13] F.H. Busse, G. Shubert (1971) Convection in a fluid with two phases. *Journal of Fluid Mechanics* **46** 801-812.

[14] C.A. Miller (1973) Stability of moving surfaces in fluid systems with heat and mass transport – II. Combined effects of transport and density difference between phases. *AIChE Journal* **19** 909-915.

[15] H.J. PALMER (1976) The hydrodynamic stability of rapidly evaporating liquids at reduced pressure. *Journal of Fluid Mechanics* **75** 487-511.

[16] A. PROSPERETTI, M.S. PLESSET (1984) The stability of an evaporating liquid surface. *Physics of Fluids* **27** 1590-1602.

[17] N. IMAISHI, M. HOZAWA, K. FUJINAWA, Y. SUZUKI (1983) Theoretical study of interracial turbulence in gas liquid mass transfer, applying Brian's linear-stability analysis and using numerical analysis of unsteady Marangoni convection. *International Chemical Engineering* **23** 466-476.

[18] S. DAVIS (1987) Thermocapillary Instabilities. *Annual Review of Fluid Mechanics* **19** 403-435.

[19] J.P. BURELBACH, S.G. BANKOFF, S.H. DAVIS (1988) Nonlinear stability of evaporating/condensing liquid films. *Journal of Fluid Mechanics* **195** 463-494.

[20] S.W. JOO, S.H. DAVIS, S.G. BANKOFF (1991) Long-wave instabilities of heated falling films: two-dimensional theory of uniform layers. *Journal of Fluid Mechanics* **230** 117-494.

[21] K. DANOV, I.B. IVANOV, Z.Z. ZAPRYANOV, E. NAKACHE, S. RAHARIMALALA (1987) Marginal stability of emulsion thin films. In: M.G. VELARDE (ed.) *Proceedings of the Conference of Synergetics, Order and Chaos*, Madrid, Spain, 13–17 October 1987, Madrid, Spain. World Scientific, Singapore, pp. 178-192.

[22] K.D. DANOV, N. ALLEBORN, H. RASZILLIER, F. DURST (1998) The stability of evaporating thin liquid films in the presence of surfactant. I. Lubrication approximation and linear analysis. *Physics of Fluids* **10** 131-143.

[23] T. GURKOV, K. DANOV, N. ALLEBORN, H. RASZILLIER, F. DURST (1998) Role of surface forces in the stability of evaporating thin liquid films that contain surfactant micelles. *Journal of Colloid and Interface Science* **198** 224-240.

[24] K.D. DANOV, V.N. PAUNOV, N. ALLEBORN, H. RASZILLIER, F. DURST (1998) Stability of evaporating two–layered liquid film in the presence of surfactant – I. The equations of lubrication approximation. *Chemical Engineering Science* **53** 2809-2822.

[25] K.D. DANOV, V.N. PAUNOV, N. ALLEBORN, H. RASZILLIER, F. DURST (1998) Stability of evaporating two–layered liquid film in the presence of surfactant – II. Linear analysis. *Chemical Engineering Science* **53** 2823-2837.

[26] V.N. PAUNOV, K.D. DANOV, N. ALLEBORN, H. RASZILLIER, F. DURST (1998) Stability of evaporating two–layered liquid film in the presence of surfactant – III. Nonlinear stability analysis. *Chemical Engineering Science* **53** 2839-2857.

[27] J.R. MAA (1967) Evaporation Coefficient of Liquids. *Industrial & Engineering Chemistry Fundamentals* **6** 504-518.

[28] A. HUANG, D.D. JOSEPH (1992) Instability of the equilibrium of a liquid below its vapour between horizontal heated plates. *Journal of Fluid Mechanics* **242** 235-247.

[29] A. HUANG, D.D. JOSEPH (1993) Stability of liquid-vapor flow down an inclined channel with phase change. *International Journal of Heat and Mass Transfer* **36** 663-672.

[30] P.N. SHANKAR, M.D. DESHPANDE (1990) On the temperature distribution in liquid–vapor phase change between plane liquid surfaces. *Physics of Fluids A* **2** 1030-1038.

[31] G. FANG, C.A. WARD (1999) Temperature measured close to the interface of an evaporating liquid. *Physical Review E* **59** 417-428.

[32] C.A. WARD, G. FANG (1999) Expression for predicting liquid evaporation flux: Statistical rate theory approach. *Physical Review E* **59** 429-440.

[33] G. FANG, C.A. WARD (1999) Examination of the statistical rate theory expression for liquid evaporation rates. *Physical Review E* **59** 441-453.

[34] C.A. WARD, D. STANGA (2001) Interfacial conditions during evaporation or condensation of water. *Physical Review E* **64** 051509.

[35] A.J.H. MCGAUGHEY, C.A. WARD (2002) Temperature discontinuity at the surface of an evaporating droplet. *Journal of Applied Physics* **91** 6406-6415.

[36] C.A. WARD, F. DUAN (2004) Turbulent transition of thermocapillary flow induced by water evaporation. *Physical Review E* **69** 056308.

[37] Y.-P. PAO (1971) Temperature and Density Jumps in the Kinetic Theory of Gases and Vapors. *Physics of Fluids* **14** 1340-1346.

[38] Y.-P. PAO (1971) Application of Kinetic Theory to the Problem of Evaporation and Condensation. *Physics of Fluids* **14** 306-312.

[39] L.D. KOFFMAM, M.S. PLESSET, L. LEES (1984) Theory of evaporation and condensation. *Physics of Fluids* **27** 876-880.

[40] C. CERCIGNANI, W. FISZDON, A. FREZZOTTI (1985) The paradox of the inverted temperature profiles between an evaporating and a condensing surface. *Physics of Fluids* **28** 3237-3240.

[41] J.W. CIPOLLA JR., H. LANG, S.K. LOYALKA (1974) Kinetic theory of condensation and evaporation. *The Journal of Chemical Physics* **61** 69-77.

[42] D. BEDEAUX, L.J.F. HERMANS, T. YTREHUS (1990) Slow evaporation and condensation. *Physica A* **169** 263-280.

[43] D. BEDEAUX, S. KJELSTRUP (1999) Transfer coefficients for evaporation. *Physica A* **270** 413-426.

[44] J.H. SIKKENK, J.M.J. VAN LEEUWEN, E.O. VOSSNACK, A.F. BAKKER (1987) Simulation of a liquid-vapor interface in an external field. *Physica A* **146** 622-633.

[45] A. RØSJORDE, D.W. FOSSMO, D. BEDEAUX, S. KJELSTRUP, B. HAFSKJOLD (2000) Nonequilibrium Molecular Dynamics Simulations of Steady-State Heat and Mass Transport in Condensation: I. Local Equilibrium. *Journal of Colloid and Interface Science* **232** 178-185.

[46] A. RØSJORDE, S. KJELSTRUP, D. BEDEAUX, B. HAFSKJOLD (2001) Nonequilibrium Molecular Dynamics Simulations of Steady-State Heat and Mass Transport in Condensation. II. Transfer Coefficients. *Journal of Colloid and Interface Science* **240** 355-364.

[47] J.A.W. ELLIOT, H.Y. ELMOAZZEN, L.E. MCGANN (2000) A method whereby Onsager coefficients may be evaluated. *The Journal of Chemical Physics* **113** 6573-6578.

[48] C.A. WARD (2002) Liquid-Vapour Phase Change Rates and Interfacial Entropy Production. *Journal of Non-Equilibrium Thermodynamics* **27** 289-303.

[49] Z. ZAPRYANOV, S. TABAKOVA (1999) "Dynamics of Bubbles, Drops and Rigid Particles". Springer, Dordrecht.

[50] G. HETSRONI (1982) "Handbook of Multiphase Systems". Hemisphere, Washington.

[51] J.C. SLATTERY (1991) "Interfacial Transport Phenomena". Springer, New York.

[52] D.D. JOSEPH (1990) "Fluid Dynamics of Viscoelastic Liquids". Springer, New York.

[53] D.A. EDWARDS, H. BRENNER, D.T. WASAN (1991) "Interfacial Transport Processes and Rheology". Butterworth-Heinemann, Boston.

[54] V.K. BADAM, V. KUMAR, F. DURST, K. DANOV (2007) Experimental and theoretical investigations on interfacial temperature jumps during evaporation. *Experimental Thermal and Fluid Science* **32** 276-292.

[55] W. WAGNER, A. KRUSE (1998) "Properties of Water and Steam". Springer, Berlin.

[56] R.C. WEAST (ED.) (1975) "Handbook of Chemistry and Physics". CRC Press, Cleveland, p. D180.